

Numerical Simulation of Internal Flow Field Characteristics for a Ducted Propeller

*Jie Gong [‡], †C.Y. Guo [‡], T.C. Wu [‡], K.W. Song [‡], and J.F. Lin [‡]

[‡]College of Shipbuilding Engineering, Harbin Engineering University, China

*Presenting author: gongjie13@hrbeu.edu.cn

†Corresponding author: guochunyu_heu@outlook.com

Abstract

The internal flow field characteristics of a ducted propeller set in a propeller open water test have been investigated numerically. Detached Eddy Simulation (DES) approach is employed to track the main features of the vortical structures of the internal wake field. The Spalart & Allmaras turbulence model and unsteady sliding mesh technique have been used in the simulations. Appropriate grid divided topology meeting the y^+ requirement and boundary conditions set to satisfy all research objectives are discussed. The results show that the numerical hydrodynamic performance results are in good agreement with the model test. The peak value of the surface pressure fluctuation occurs in the blade passing frequency (BPF) and its multiples in the frequency domain. DES model can effectively simulate the different vortex structures of the ducted propeller, such as shear layer vortices of the duct, blade tip vortices, blade shedding vortices and blade root vortex. Tip vortex structures perform strong deformation due to the interaction between the duct and the propeller. The morphology of tip vortex changes and the vorticity distribution covers a larger area of the inner surface of the duct. All above contributes to the recovery of the propeller wake vortex energy and increases the efficiency of the propulsion.

Keywords: Ducted propeller, DES, Pressure fluctuation, Vortex structure.

1. Introduction

Ducted propeller is widely used in the propulsion system for various engineering vessels. The duct could provide protection for the propeller and improve the efficiency of the propulsion system. In addition, the ducted propeller gets a better performance for cavitation and radiation noise, especially in heavy load conditions. Research [1] shows that the circulation flow that distributes near the inner surface of the duct is the essential reason for the production of duct thrust, while the duct is helpful to recover the vortex energy induced by the propeller. In order to further understand the mechanism of the hydrodynamic performance of the ducted propeller, the flow characteristics of the internal flow field of ducted propeller (especially vortex characteristics) are necessary analyzed.

Most of the early numerical calculations are based on potential flow theory [2]-[3], Su et al. [4] and Xie et al. [5] has calculated the hydrodynamic performance and internal flow field of ducted propeller by using the panel method theory which is based on velocity potential. It is concluded that the computational efficiency of potential flow method is considerable, but it is difficult to simulate the complex flow accurately. Recently, numerous numerical methods based on viscous flow have been applied in the simulations for ducted propellers [6]-[9]. Based on solving the Reynolds-averaged Navier-Stokes equations (RANS), the flow field around the ducted propeller and the characteristics of the wake vortex are predicted by Hu et al. [10] and Shi et al. [11]. Bhattacharyya et al. performed extensive studies on predicting the

hydrodynamic performance of ducted propeller, including the manner in which different types of ducts affect propeller performance [12], scale effects of the ducted propellers [13], and the application of computational fluid dynamics (CFD) in the design of ducted propellers [14]. Gaggero et al. [15] used the RANS method to perform numerical predictions on cavitating tip vortices in ducted propellers, and the meshing and refinement topology used in this study are highly valuable as a reference for numerical studies as they attempted to capture the details of the flow field.

In this paper, numerical simulation of ducted propeller for open-water test is performed basing on the detached eddy simulation (DES) method. In order to confirm the accuracy and reliability of numerical calculation, the calculated hydrodynamic performance is verified by comparing with model test results. The detailed numerical model of grid type, turbulence model and computational methods has been described. The objective of this study focus on the analysis of the distribution characteristics of the internal flow field of the ducted propeller, as well as the structural composition, morphology and distribution characteristics of vortices of internal flow fields following the effects of complex interferences.

2. Computational details

2.1 Governing equations

The numerical simulations of viscous flow field is performed by the integration of the RANS equation. The motion of incompressible Newton fluids is integrated with the continuity equation and momentum conservation equation [16] as follows:

$$\frac{\partial u_i}{\partial x_i} = 0 \quad (1)$$

$$\frac{\partial(\rho u_i)}{\partial t} + \frac{\partial}{\partial x_j}(\rho u_i u_j) = \frac{\partial p}{\partial x_j} + \frac{\partial}{\partial x_j}(\mu \frac{\partial u_i}{\partial x_j} - \overline{\rho u_i u_j}) + S_j \quad (2)$$

where u_i and u_j denote the time-averaged values of velocity components ($i, j = 1, 2, 3$), p denotes time-averaged pressure, μ denotes the dynamic viscosity coefficient, $\overline{\rho u_i u_j}$ denotes the Reynolds stress term, and S_j denotes the generalised source term of the momentum equation.

The DES model is a hybrid numerical model that combines the strengths of both RANS and LES methods. In all DES simulations, the Spalart & Allmaras one-equation [17] turbulence model is employed to resolve turbulence structures in the wake. The finite volume based segregated flow solver of the STAR-CCM+ CFD code is utilised to simulate the flow-field characteristics of the internal vortices generated by the ducted propeller under various advance coefficients. In the DES simulation, the SIMPLE algorithm is adopted to solve the pressure-velocity coupling equation. Specifically, convection, diffusion, and time terms are discretised by using the 2nd order upwind scheme, central differencing scheme, and 2nd order implicit time discretisation, respectively. In the unsteady DES simulation, the Courant-Friedrichs-Lewy (CFL) condition is used to balance the temporal and the spatial scales.

2.2 Computational conditions

The propeller is a constant-pitch 4-bladed propeller with a diameter of $D = 0.240$ m, a hub ratio of 0.190, and a propeller area ratio of 0.417. The Wageningen 19A duct is integrated with a tip clearance of 2 mm. The geometry of the studied ducted propeller is shown in Figure 1. An O-xyz Cartesian coordinate system with the origin O located at the geometrical centre of the propeller is built in the simulation. The positive direction of the x-axis is defined as the uniform inflow direction, while the positive directions of the y and z axes are determined by the right-hand rule.

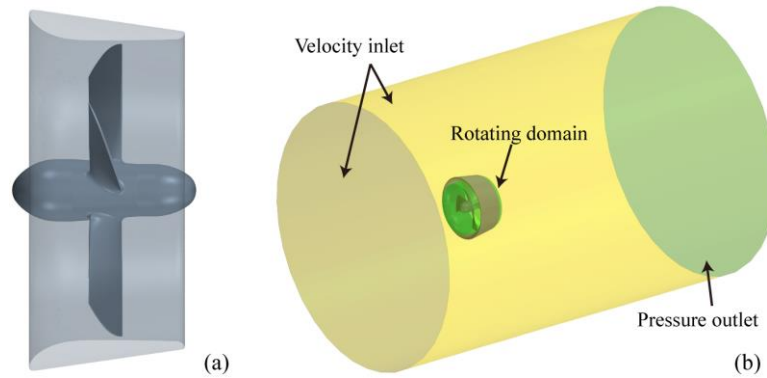


Figure 1. Geometric model and calculation domain

The computational domain is a cylinder with a diameter of $8D$, and extends $2D$ upstream and $8D$ downstream from the origin O , respectively. The sliding mesh method is used in the simulation of the propeller rotating motion, hence, the computational domain is divided into static and rotating sub-domains. The boundary conditions of the computational domain are set as follows: the inlet and the side boundary of the cylinder are both set to the velocity inlet; the outlet is set to the pressure outlet; the surfaces of the propeller and the duct are set to the no-slip wall.

2.3 Mesh characteristics

A proper discretisation of the computational domain is extremely important to improve the accuracy of the numerical simulation. It is necessary for the cell size of the computational domain to transition in a gradual manner to avoid numerical dissipations. In the study, the rotational sub-domain is discretised by using a polyhedral mesh while the static sub-domain is discretised by using a trimmed mesh.

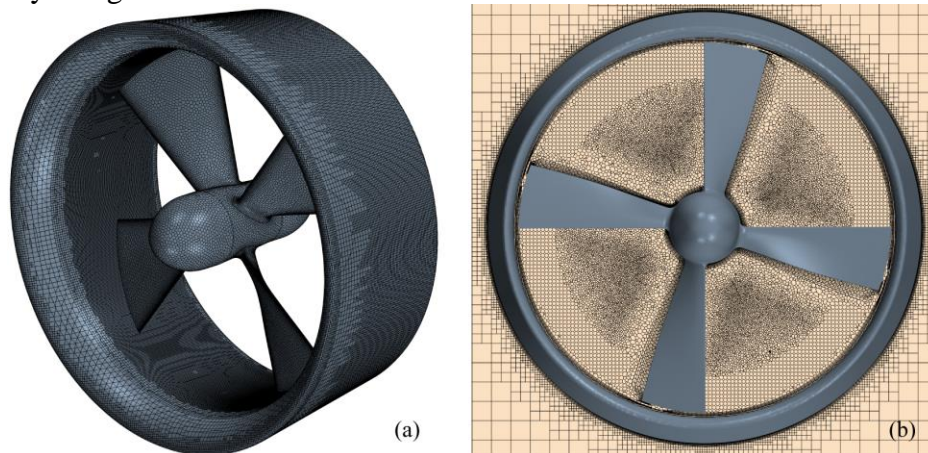


Figure 2. Surface mesh of ducted propeller and details of mid-ship section

The meshes of two sub-domains possess a same base size (BS) of 0.1 m. A volume refinement (size = 2.5% BS) is implemented in the annular cylindrical region of the blades' tips, while a gap refining region with an even finer grid size (size = 1.25% BS) is employed in the gap between the blades' tips and the duct (shown in Figure 2). The blade surfaces are refined along the feature lines of the leading and trailing edges (size = 0.25% BS). In addition, a hub vortex refining region is set up behind the hub to capture the formation and evolution of the hub vortex. The total number of cells of the computational domain corresponds to 9.51 million while the static and rotational sub-domains account for 7.36 million and 2.15 million. In order to satisfy the requirements of the DES algorithm, the y^+ value of the walls is restricted to $y^+ < 1$.

3. Results and discussion

3.1 Verification of hydrodynamic performance

The hydrodynamic coefficients of ducted propellers are defined as follows:

$$J = \frac{V_x}{nD} \quad (3)$$

$$K_{tp} = \frac{T_p}{\rho n^2 D^4}, K_{td} = \frac{T_d}{\rho n^2 D^4} \quad (4)$$

$$K_q = \frac{Q_0}{\rho n^2 D^5} \quad (5)$$

$$\eta_0 = \frac{J}{2\pi} \frac{K_{tp} + K_{td}}{K_q} \quad (6)$$

where, J is the advanced coefficient, V_x is the local axial velocity, n is the rotate speed, D is the diameter of the propeller, T_p and T_d are the thrusts of propeller and duct, Q_0 is the torque of propeller, ρ is the density of fluid. K_{tp} and K_{td} are the thrust coefficients of propeller and duct, respectively. K_q is the torque coefficient of propeller and η_0 is the efficiency of the ducted propeller.

Three advance coefficients, 0.3, 0.4 and 0.5, were chosen to allow for a comparison between different loads. A constant rotational speed, $n = 11$ revolutions per second (RPS) was selected in the simulations, and the time step was set to 1° /step. The fluid density was kept constant at $\rho = 997.56 \text{ kg m}^{-3}$, and the Reynolds number is the same as that of the model experiment, i.e. $Re = 3.5 \sim 3.6 \times 10^5$.

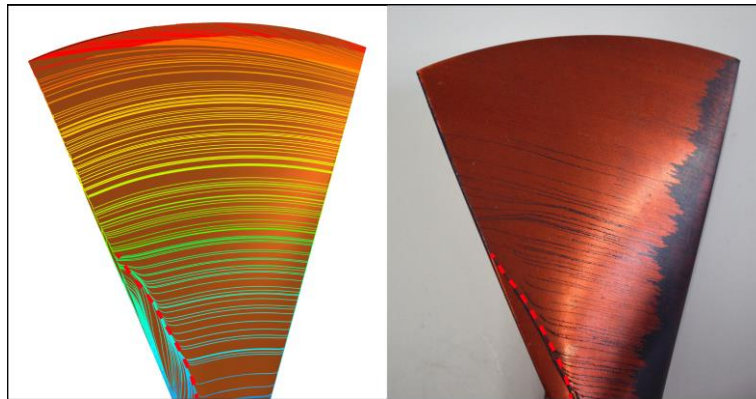


Figure 3. Streamlines of blade surface; Left: CFD, Right: EFD

Compared with the experiment results, the maximum relative error among all coefficients is the duct thrust coefficient, which has reached 4.42%. The periodic rotation of the impeller has caused the thrust fluctuation of duct. All thrust coefficients, torque coefficients of the propeller are in good agreement with the experimental results, the errors are within 3%. Results above show that the computational accuracy of the numerical model is acceptable, and the analysis of the characteristics of the internal flow field and vortex characteristics are of relative reliability.

Table1. Comparison of numerical calculation (CFD) and model test results (EFD)

J	K_{tp}			K_{td}			$10K_q$		
	CFD	EFD	Er.(%)	CFD	EFD	Er.(%)	CFD	EFD	Er.(%)
0.3	0.2017	0.1985	1.61	0.0842	0.0881	-4.42	0.3369	0.3401	-0.94
0.4	0.1806	0.183	-1.31	0.0565	0.0581	-2.75	0.308	0.316	-2.53
0.5	0.1615	0.1664	-2.94	0.0287	0.0279	2.86	0.2876	0.2915	-1.33

3.2 Internal flow field characteristics

Typical profiles are selected to analyze the characteristics of the internal flow field. Two cross sections (y - z plane) are selected at the front disk ($x=-0.5R$) and the back disk ($x=0.3R$) in the

internal region, and all the coordinates are normalized by the radius of the propeller. The transient induced axial velocity and vorticity distribution are analyzed in detail.

The presence of the duct enhanced the suction effect in front of the propeller, and the axial speed in the front disk changed obviously. Analysis along the radial direction, the axial induced velocity (V_{x-in}) increased first and then decreased (Figure 4 (a)), which is caused by the retardant of the duct surface and the hub. The axial induced velocity has shown obvious periodicity fluctuation for different radius in the front disk during one period. There are 4 peaks of the induced axial velocity for all the radius ($0.4R$, $0.6R$ and $0.8R$), which is the same with the number of blades. In addition, as closer to the outside of the disk, the induced velocity fluctuation amplitude is larger, and the position of $0.8R$ generates the most intense fluctuation obviously.

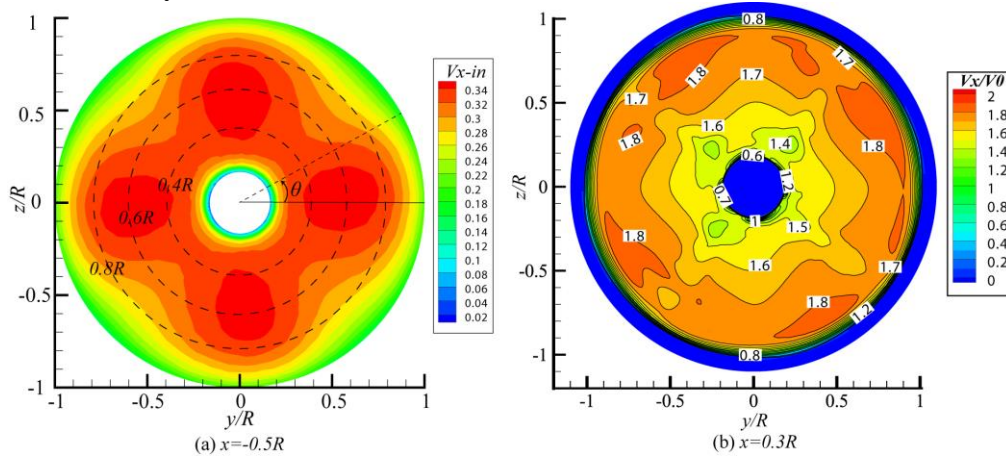


Figure 4. Axial velocity distribution of the front and back disks ($x=-0.5R$ and $x=0.3R$)

The dimensionless axial velocity (V_x/V_0) distribution for the back disk ($x=0.3R$) is shown in Figure 4 (b). It can be observed that acceleration of the blades is reflected in the range of $0.5-0.8R$, and the transient axial velocity distributes in the range of $1.4\sim 1.8$. The vorticity distribution could reflect the composition of the internal vortex system of the duct propeller. The shear flow of the inner surface of the duct generates shear layer vortices, and the shear layer vortices show a ring shape in the cross section. On the other hand, the vortex system induced by the propeller are described as follows: blade tip vortex (Figure 5(a)-I), blade shedding vortex (Figure 5(a)-II) and blade root vortex (Figure 5(a)-III), and the vortices cores distributed near the maximum value of vorticity. Furthermore, the turbulent viscosity (Figure 5(b)) in the back disk reflects the eddy diffusion motion. It is obvious that the turbulent viscosity is larger in the blade tip and root zones, and which means the turbulent viscosity distribution is consistent with the vortex distribution characteristics.

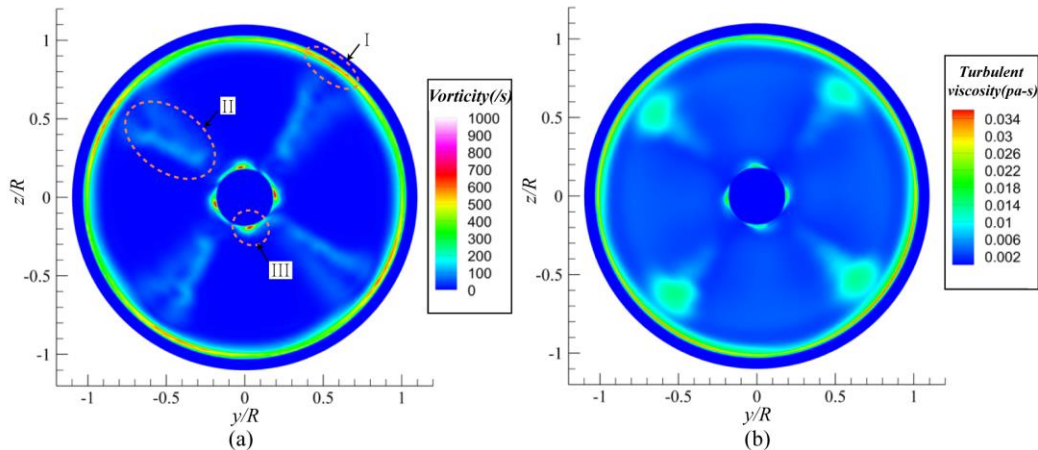


Figure 5. Typical quantities distributions of the back disk($x=0.3R$); (a) vorticity; (b) turbulent viscosity

Meanwhile, by setting the probe P_1 at the $x=0$ cross section of the inner surface of the duct, the variation of pressure pulsation at P_1 position for operation conditions is monitored. For the time domain, there are 4 peak and valley pressure value during one period, and the pulsation amplitude is directly related with the blade position. The flow field changes sharply and the hydrodynamic performance of the ducted propeller is unsteady. For the frequency domain, the pressure peaks appear at the blade passing frequency (BPF) and its multiples, the continuous peaks are progressively shifted with respect to the integer BPF. The pressure pulsation characteristics of the inner surface of the duct relate to the actual working conditions of ducted propellers.

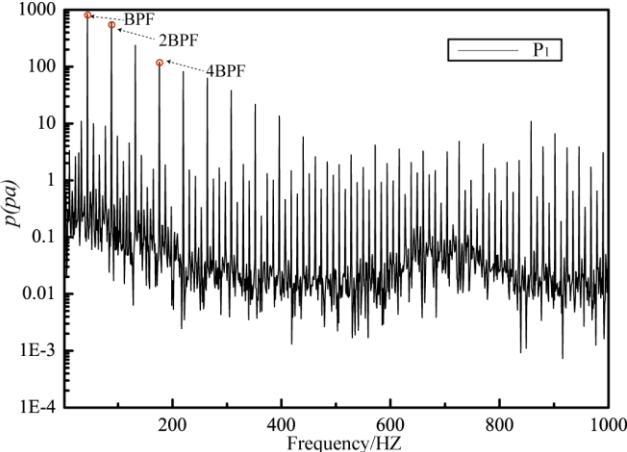


Figure 6. Pressure fluctuation of probe P_1 in the frequency domain

3.3 Vortex characteristics analysis

The vortex characteristics of internal flow fields and its distribution affect the hydrodynamic performance of the ducted propeller directly. The horizontal section ($z=0$) is selected to analyze the distribution of velocity and vorticity along the stream direction. As shown in Figure 7, the acceleration effect of the ducted propeller on the passing flow is obvious in the velocity field. Because of the fluid viscous action, there is a low velocity zone distributing at the trailing edge of the duct. On the other hand, there distributes large areas of vorticity near the duct inner surface (Figure 8), the vortices are generated by the pressure difference before and after the blade surfaces. The strong interaction between the propeller and the duct has made the vortices structures more complicated (Figure 8-I). It is relatively clear to recognize the blade root vortex (Figure 8-II) and the hub vortex (Figure 8-III). In addition, the shear layer vortex of the outer surface and the internal vortices interfere with each other near the duct tailing region, and the vortex energy transfer to the downstream. There exists continuous elliptical vorticity distributions (Figure 8-IV) in the near wake field.

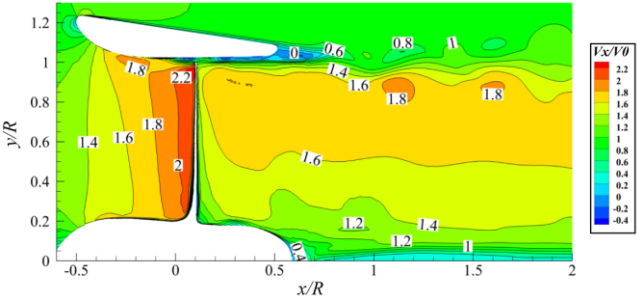


Figure 7. Instantaneous velocity distribution of the horizontal section ($z=0$)

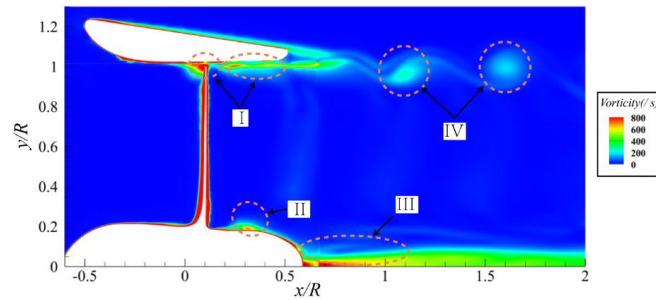


Figure 8. Instantaneous vorticity distribution of the horizontal section ($z=0$)

The volume render method is employed to analyze the instantaneous spatial vorticity distributions. As shown in Figure 9, four flake blade shedding vortices are generated near the blade trailing edges, and the energy diffuses rapidly in the stream. The different root vortices develop spirally and gather near the hub region gradually. The tip vortex distributes on the inner surface of the duct, and the morphology of the tip vortex has changed significantly. There is a larger area of vortices distributing on the inner wall, which causes stronger circulations and produces the hydrodynamic thrust of the duct.

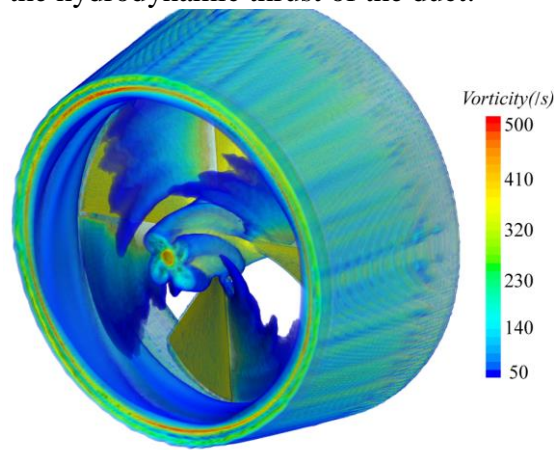


Figure. 9 Three-dimensional vorticity distribution in internal flow field of ducted propeller

The internal characteristics of tip vortex deformation are discriminated. The contour projection is in the shape of “W”, and there are two eddy centres in the internal flow field, which is obviously different from the vorticity distribution of a non-ducted propeller. Furthermore, it is found that the vorticity value of two eddy centres gradually decreased along the flow direction.

4. Conclusion

The DES method has been implemented in the simulations of the internal flow field characteristics and vortex structures of the ducted propeller. The results indicate that DES method can obtain a reasonable numerical accuracy and capture the flow characteristics well. The conclusions are as follows:

1. The internal flow field vortex system of the ducted propeller includes the shear layer vortex of the duct, the blade tip vortex, shedding vortex, root vortex and the hub vortex.
2. The existence of the duct directly affects the distribution of propeller tip vortex. A larger area of vortices distributing on the inner wall of the duct is helpful to recover the vortex energy so as to improve the propulsion efficiency.

Acknowledgements

This project was supported by the National Natural Science Foundation of China (Grant Nos. 51379043, 51209048 and 51409063), and thanks for the technical support provided by Dr. Xu Yongze and Dou Pengfei of Siemens Ltd. China.

Reference

- [1] Go, J.S., Yoon, H.S. and Jung, J.H. (2017) Effects of a duct before a propeller on propulsion performance. *Ocean Engineering*, 136, 54-66.
- [2] WANG, G.Q. and LIU, X.G. (2006) Prediction of unsteady performance of ducted propellers by potential based panel method, *Journal of Ship Mechanics*, 10(1): 36-42.
- [3] HU, J., HUANG, S., MA, C. and XIE, X.S. (2009) Several Influence Factors for the Inner Flow Field of Ducted Propeller, *JOURNAL OF TIANJIN UNIVERSITY*, 42(4):340-344.
- [4] SU, Y.M., LIU, Y.B., SHEN, H.L. and DOU, F.X. (2012) Surface panel method-based numerical calculation for predicting ducted propeller performances, *JOURNAL OF HUAZHONG UNIVERSITY OF SCIENCE AND TECHNOLOGY. NATURE SCIENCE*, 08:57-61.
- [5] XIE, X.S., HUANG, S., HU, J., and MA, C. (2009) Inner flow field calculations for ducted propellers, *JOURNAL OF HARBIN ENGINEERING UNIVERSITY*, 01: 7 -12.
- [6] ZHOU, J.W., LI, F.Z. and MEI, L. (2017) Peak efficiency analysis of non-cavitation ducted propeller, *Journal of Harbin Institute of Technology*, 04: 149-155.
- [7] LIU, Y.B., SHU, Y.M., ZHAO J.X. and ZHANG, H. (2014) Optimal design of a ducted propeller based on the circulation theory and pump theory, *JOURNAL OF HARBIN ENGINEERING UNIVERSITY*, 11: 1307-1313.
- [8] RAO, Z.Q., LI, W. and YANG, J.C. (2014) The Effect of Stator Parameters on Performance of Ducted Propeller with Pre-swirl Stators, *Journal of Shanghai Jiaotong University*, 11:1307-1313.
- [9] HU, J., WANG, N. and HU, Y. (2017) Performance comparison of accelerating duct and decelerating duct, *Journal of Beijing University of Aeronautics and Astronautics*, 02: 240-252.
- [10] HU, J., WANG, N. and HU, Y. (2017) Numerical Study on the Hydrodynamic performance of Ducted Propellers, *JOURNAL OF HARBIN ENGINEERING UNIVERSITY*, 06:1-7.
- [11] SHI, L.P., XIONG, Y., YANG, Y. and WANG, B. (2016) Numerical simulation of the flow around a ducted propeller using Reynolds-averaged Navier-Stokes equations, *JOURNAL OF HARBIN ENGINEERING UNIVERSITY*, 03: 344-348.
- [12] Bhattacharyya, A., Krasilnikov, V. and Steen, S. (2016) Scale effects on open water characteristics of a controllable pitch propeller working within different duct designs, *Ocean Engineering*, 112: 226-242.
- [13] Bhattacharyya, A., V. Krasilnikov, and Steen, S. (2015) Scale Effects on a 4-Bladed Propeller Operating in Ducts of Different Design in Open Water, *Fourth International Symposium on Marine Propulsors smp'15, USA*.
- [14] Bhattacharyya, A., V. Krasilnikov, and Steen, S. (2016) A CFD-based scaling approach for ducted propellers, *Ocean Engineering*, 123:116-130.
- [15] S. Gaggero, G. Tani, M. Viviani, and F. Conti. (2014) A study on the numerical prediction of propellers cavitating tip vortex, *Ocean Engineering*, 92:137-161.
- [16] GONG, J., GUO, C.Y. and ZHANG, H.P. (2017) Numerical Analysis of Impeller Flow Field of Waterjet Self-Propelled Ship Model, *Journal of Shanghai Jiaotong University*, 03:326-331.
- [17] Philippe R. Spalart. (2009) Detached-Eddy Simulation, *Annual Review of Fluid Mechanics*, 41:181-202.